Direct ab initio dynamics study of the OH + HOCO reaction

ARTICLE *in* THE JOURNAL OF PHYSICAL CHEMISTRY A · JULY 2005

Impact Factor: 2.69 · DOI: 10.1021/jp051458w · Source: PubMed

3 AUTHORS, INCLUDING:

James T Muckerman
Brookhaven National Laboratory
237 PUBLICATIONS **6,436** CITATIONS

Direct ab Initio Dynamics Study of the OH + HOCO Reaction

Hua-Gen Yu* and James T. Muckerman

Department of Chemistry, Brookhaven National Laboratory, Upton, New York 11973-5000

Joseph S. Francisco†

Department of Chemistry, Purdue University, West Lafayette, Indiana 47907

Received: March 21, 2005; In Final Form: April 19, 2005

The reaction between OH and HOCO has been examined using the coupled-cluster method to locate and optimize the critical points on the ground-state potential energy surface. The energetics are refined using the coupled-cluster method with basis set extrapolation to the complete basis set (CBS) limit. Results show that the OH + HOCO reaction produces H_2O + CO_2 as final products and the reaction passes through an HOC(O)OH intermediate. In addition, the OH + HOCO reaction has been studied using a direct dynamics method with a dual-level ab initio theory. Dynamics calculations show that hydrogen bonding plays an important role during the initial stages of the reaction. The thermal rate constant is estimated over the temperature range 250−800 K. The OH + HOCO reaction is found to be nearly temperature-independent at lower temperatures, and at 300 K, the thermal rate constant is predicted to be 1.03×10^{-11} cm^3 molecule^{-1} s^{-1}. In addition, there may be an indication of a small peak in the rate constant at a temperature between 300 and 400 K.

I. Introduction

The HOCO radical is a key intermediate produced in atmospheric and combustion processes. It plays an important role in the oxidation of CO to CO_2 involving OH radicals[1−6] via

$$\begin{array}{c} \mathrm{OH + CO \rightarrow HOCO^* \rightarrow H + CO_2} \\ \downarrow \mathrm{M} \\ \mathrm{HOCO} \end{array}$$

The spectroscopic characterization of HOCO has provided[7−13] experimental probes of the radical. Moreover, pressure-dependent studies by DeMore[14] and others[11,15−17] suggest that there is an appreciable abundance of stabilized HOCO in atmospheric and combustion environments. An examination of the elementary chemical reactions involved in removal mechanisms for the HOCO radical is important. The reaction of HOCO with O_2 has attracted considerable attention, as well as its reaction with NO. Experimental[18,19] and theoretical studies[20] show that both these reactions proceed through the formation of an adduct. Recent experimental studies[21] have isolated the adduct produced from the HOCO + NO reaction. The HOCO + NO reaction is considered a classic radical−radical reaction. The reaction of OH + HOCO is also a radical−radical reaction and could be equally important in removing HOCO radicals from atmospheric and combustion environments. Our survey of atmospheric and combustion models shows that this reaction has not been included. Our survey of the literature showed that the reaction has not been studied either experimentally or theoretically, which is surprising, since in the OH + CO reaction that produces the HOCO radical, one has to consider the roles that the secondary reaction of the radical with OH might play in influencing the resulting abundance of CO_2, which is a product of the OH + CO reaction and the OH + HOCO reaction.

This paper presents the first study of the OH + HOCO reaction. The essential critical points on the potential energy surface are examined, and a direct ab initio dynamics study is also carried out to understand the detailed OH + HOCO reaction mechanism. Rate constants are determined for the OH + HOCO reaction that can be used to assess the reaction's significance in atmospheric and combustion processes.

II. Computational Method

The potential energy surface for the OH + HOCO reaction was explored with two levels of theory. The first level of theory used in preliminary searches of global minima and transition states was the quadratic configuration interaction with single and double excitations method (QCISD)[22] using the Dunning correlation consistent cc-pVDZ basis set.[23,24] Full geometry optimizations were performed for all the structures using Schlegel's method[25] with tolerances to better than 0.001 Å for bond lengths and 0.01° for angles, with a self-consistent field convergence of at least 10^{-9} on the density matrix. The residual rms (root-mean-square) force was less than 10^{-4} au. The maximum residual force was 0.00016 au for open-shell reactants and 0.00018 au for transition states. Vibrational frequency calculations were performed to determine whether the critical points that were located were either minima or transition states on the potential energy surface, that is, all positive frequencies (minima) or one imaginary frequency (first-order saddle points). The Hessians from these optimizations were then used to search for the global minima and transition states using the second level of theory, the coupled-cluster method including single and double excitations along with a perturbation correction for the triple excitations (CCSD(T)).[26,27] The eigenvalue following method was used with this method along with the Hessian from

* E-mail: hgy@bnl.gov.
† E-mail: francisc@purdue.edu.

10.1021/jp051458w CCC: $30.25
Published on Web 05/20/2005

the QCISD optimization. Vibrational frequency calculations were repeated to confirm that the critical points located were either minima or transition states on the potential energy surface. These calculations were carried out at the CCSD(T)/cc-pVDZ level of theory. To improve the energetics, optimizations were carried out with the CCSD(T) method using the larger cc-pVTZ basis set. In addition, a single-point energy calculation was performed at the CCSD(T)/cc-pVTZ geometries using the CCSD(T) method with the cc-pVQZ basis set. Because spin contamination may produce inaccurate total energies when performing these calculations, the total spin expectation value $\langle S^2 \rangle$ was closely monitored. The largest preannihilation deviation from the expected $\langle S^2 \rangle$ value of 0.75 for open-shell species was less than 3%, and therefore, spin contamination was considered negligible for the OH + HOCO reaction system. The three-parameter complete-basis-set extrapolation procedure of Peterson et al.[28] was used to refine the energetics

$$E(n) = E(\infty) + A \exp[-(n-1)] + B \exp[-(n-1)^2]$$

The dynamics calculations were carried out using the *DualOrthGT* program.[29] Because the procedure has been well-described elsewhere,[29,30] we will not provide many details here. Briefly, trajectories were propagated with a time step of 0.32−0.43 fs for a set of randomly sampled initial conditions[29,31] for a given temperature (T). The orientation, rotational energy, vibrational quantum numbers and phases, and relative collision velocity of reactants were selected according to the canonical ensemble at T. The initial velocity is given by[32,33]

$$v_r = \sqrt{\frac{2E_{rel}}{\mu}}$$

where μ is the reduced mass of OH and HOCO and E_{rel} is the relative kinetic energy obtained by iteratively solving

$$1 - (1 + E_{rel}/k_B T) \exp(-E_{rel}/k_B T) - \xi_r = 0$$

Here, ξ_r is a random number uniformly distributed in (0, 1), and k_B is the Boltzmann constant. The initial center-of-mass distance between the OH and HOCO reactants was set to $\rho_0 = \sqrt{R_0^2 + b^2}$ with $R_0 = 12.5a_0$, where $b = \xi^{1/2} b_{max}$ is the impact parameter and ξ is another random number uniformly distributed in (0, 1), and $b_{max} = 9.5a_0$ is the maximum impact parameter. All trajectories were terminated either when the reactants had formed an HOC(O)OH intermediate complex or when the center-of-mass distance between the collision partners became larger than $7.0a_0$ in nonreactive trajectories. In this work, we have assumed that all trajectories forming intermediate complexes would eventually dissociate into the products. This assumption is based on the fact that the transition barrier for dissociation lies well below the reactants. Therefore, the probability for the reverse reaction of HOC(O)OH is negligible. This assumption results in a substantial savings in the computational cost but makes it impossible to analyze the product distributions. In addition, during the trajectory propagation, the fragments of the collision system were monitored using graph theory[34,35] as described in our previous work.[30]

In the quasi-classical trajectory (QCT) calculations, a direct ab initio dynamics approach was used in order to avoid the difficulty of constructing an analytic potential energy surface. The forces used in the QCT were evaluated on the fly, based on a dual-level ab initio potential energy surface. The surface is obtained by the "scaling all correlation" (SAC) method of Truhlar et al.,[36−38] that is

$$E_{SAC} = E_{UHF} + \frac{E_{UMP2} - E_{UHF}}{F}$$

where E_{UHF} and E_{UMP2} are the unrestricted Hartree−Fock and second-order UMP2 energies with the 6-31G(d) basis set. The global scaling factor F was determined to be 1.08 by minimizing the rms errors of the relative SAC energies of the stationary points relative to the CBS−∞ results. Here, the well depth of the HOC(O)OH minimum and its dissociation barrier height were used, because these two points are most important in the dynamical studies of the reaction. In addition, to get a correct initial guess of the electronic state of the reactants for each trajectory, we have used the CAS(4,4)/6-31G(d) method to produce the initial electronic wave function at the beginning of every trajectory propagation. Otherwise, the initial electronic wave function may correspond to an excited state because of a large separation of two open-shell radicals. We note that the scaling factor, F, is larger than unity, indicating that the computed UMP2 correlation energy is being decreased, but we have found that often the MP2 level of theory overestimates the variation of the correlation energy over a potential energy surface. All electronic structure calculations were performed using the *Gaussian 03* program.[39]

Thermal rate constants[31−33] are calculated as

$$k(T) = g_e \pi b_{max}^2 \left(\frac{8k_B T}{\pi \mu}\right)^{1/2} P_r$$

with the reaction probability

$$P_r = N_r/N$$

and where $g_e = {}^1/_4$ is the electronic statistical factor for the reaction. Here, N_r and N are the number of reactive trajectories and the total number of trajectories, respectively, at the temperature T. The statistical errors of the calculated rate constants are given by

$$\Delta k(T) = k(T) \left(\frac{N - N_r}{N_r N}\right)^{1/2}$$

III. Results and Discussion

A. Potential Energy Surface for the OH + HOCO Reaction. The products of the OH + HOCO reaction are H_2O and CO_2. There are two routes to the formation of these products. One route is by direct abstraction of the hydrogen from the HOCO radical by OH. The second route is by the addition of the OH radical to HOCO to form the HOC(O)OH intermediate that can be stabilized or undergo elimination to generate the products H_2O and CO_2. The direct abstraction and addition−elimination pathways are illustrated in Figure 1.

The direct abstraction of hydrogen from HOCO by OH involves the approach of the incoming oxygen atom in OH along the HO axis of HOCO. Three atoms are involved in the bond-breaking and bond-forming processes. Preliminary searches at low levels of theory (HF/6-31G*) for the transition state for this process resulted in the location of a saddle point. Higher levels of theory, however, failed to locate the transition state. Instead, as the OH radical approached along the HO axis of HOCO, it moved off-axis to add to the carbon. Thus, at high levels of theory, the preliminary calculations suggested that addition to form the HOC(O)OH intermediate is the more important route compared to the direct hydrogen abstraction pathway.

TABLE 1: Geometries[a] for the HOC(O)OH Comformers

	(cis, cis)		(cis, trans)		(trans, cis)		(trans, trans)	
coordinate	cc-pVDZ	cc-pVTZ	cc-pVDZ	cc-pVTZ	cc-pVDZ	cc-pVTZ	cc-pVDZ	cc-pVTZ
O′H	0.971	0.965	0.971	0.965	0.970	0.964	0.967	0.961
CO′	1.346	1.340	1.363	1.357	1.346	1.339	1.365	1.358
CO″	1.211	1.205	1.203	1.197	1.203	1.197	1.196	1.190
CO	1.346	1.340	1.346	1.339	1.363	1.357	1.365	1.358
OH	0.971	0.965	0.970	0.964	0.971	0.965	0.967	0.961
O″CO′	125.9	125.7	125.3	125.2	125.3	124.3	122.2	122.0
CO′H	104.5	105.3	105.0	105.8	107.0	108.1	111.0	112.1
COH	104.5	105.3	107.0	108.1	105.0	105.8	111.0	112.0
O″CO′H	0.0	0.0	0.0	0.0	180.0	180.0	180.0	180.0
HOCO″	0.0	0.0	180.0	180.0	0.0	0.0	180.0	180.0

[a] Calculated at the CCSD(T) level of theory.

TABLE 2: Conformational Analysis Energetics for HOC(O)OH

			CCSD(T) total energy			relative energetic		
structure	τ(HO′CO″)	τ(HOCO″)	cc-pVDZ	cc-pVTZ	cc-pVQZ	cc-pVDZ	cc-pVTZ	cc-pVQZ
(cis, cis)	0.0	0.0	−264.385540	−264.656161	−264.740381	0.0	0.0	0.0
(cis, trans)	0.0	180.0	−264.382057	−264.653304	−264.737611	2.2	1.8	1.7
(trans, cis)	180.0	0.0	−264.382058	−264.653304	−264.737611	2.2	1.8	1.7
(trans, trans)	180.0	180.0	−264.365890	−264.638503	−264.723050	12.3	11.1	10.9
[(cis, cis) → (cis, trans)]‡	0.0	91.0 (90.7)[a]	−264.367993	−264.639372	−264.723588	11.0	10.5	10.5

[a] Optimized dihedral angle; the number in parentheses is the CCTD(T)/cc-pVTZ result.

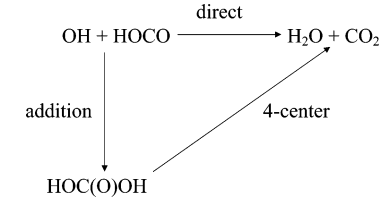

Figure 1. Reaction scheme for the OH + HOCO reaction.

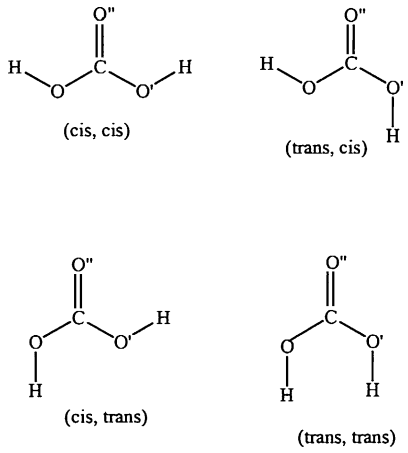

Figure 2. Conformations of the HOC(O)OH intermediate.

B. Formation of the HOC(O)OH Intermediate. The HOC(O)OH intermediate formed from the addition of OH to HOCO appears in four conformations, as shown in Figure 2. There are two dihedral angles that characterize the conformations: the τ(HOCO″) and τ(O″CO′H) dihedral angles. When both τ(O″CO′H) and τ(HOCO″) angles are 0°, it is a (cis, cis) conformation. On the other hand, the (trans, trans) conformation has a value of 180° for the τ(O″CO′H) and τ(HOCO″) angles. All four conformations have been optimized at the CCSD(T)/cc-pVDZ and CCSD(T)/cc-pVTZ levels of theory. The complete listing of geometrical parameters for each conformation is given in Table 1. Of the four conformations, the most stable is the (cis, cis) as shown in Table 2. The least stable structure is the (trans, trans). The energy separation between these two conformations is 10.9 kcal mol^{-1} at the CCSD(T)/cc-pVQZ//CCSD(T)/cc-pVTZ level of theory. The (cis, trans) and (trans, cis) conformations are structurally isomorphic. At all levels of theory, they are energetically the same. At the CCSD(T)/cc-pVQZ//CCSD(T)/cc-pVTZ level of theory, these structures are only 1.7 kcal mol^{-1} above the (cis, cis) configuration. However, to move from the (cis, cis) structure to the (cis, trans) conformation requires overcoming a 10.9 kcal mol^{-1} rotational barrier as a result of the strong hydrogen bonding that forms between the acidic hydrogen of the OH group and the carbonyl oxygen in the HOC(O)OH intermediate. Vibrational frequency calculations performed on all four conformations show all positive frequencies, thus indicating that these structures are stable minima, but the global minimum structure is the (cis, cis) conformer.

Preliminary searches for a reaction barrier for the addition of OH to the HOCO radical to form the HOC(O)OH intermediate failed to locate one. The well depth for the formation of the (cis,cis)-HOC(O)OH conformation is −108.9 kcal mol^{-1} at the CCSD(T)/cc-pVQZ//CCSD(T)/cc-pVTZ level of theory.

C. Formation of H_2O + CO_2 from the HOC(O)OH Intermediate. The dissociation of the HOC(O)OH intermediate into H_2O + CO_2 can only occur from the (cis, trans) or (trans, cis) conformation, not from the lowest-energy (cis, cis) conformation. In the (cis, trans) conformation, the O″CO′H atoms are in a position for the HOC′(O)OH intermediate to proceed through the four-center transition state shown in Figure 3 to produce H_2O and CO_2 products. The geometric parameters for the transition state are given in Table 3 and those for the HOC(O)OH (cis, trans) conformation are also provided for comparison. The CO bond length in this transition state is 1.658 Å, and the OH bond is extended to 1.245 Å, which is 23.8% longer than the CO bond and 29.0% longer than the OH bond, respectively, in the (cis, trans)-HOC(O)OH intermediate. The CO′H angle is quite small, 79.7°, while the OCO′ angle is 93.3°. These structural changes suggest that the HOC(O)OH → H_2O + CO_2 transition state is a relatively late transition state. A vibrational frequency calculation at the CCSD(T)/cc-pVDZ level of theory revealed that the transition state is a first-order saddle point with an imaginary frequency of 1780i. As mentioned above, the (cis, cis)-HOC(O)OH conformation once produced

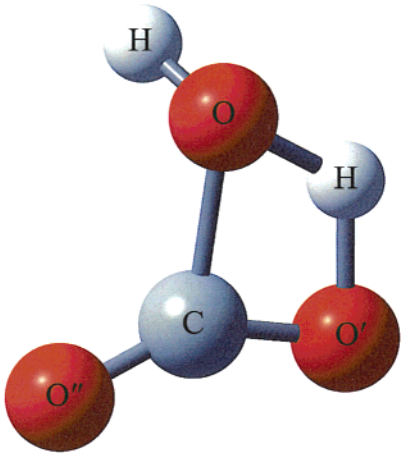

Figure 3. Transition state structure for the dissociation of HOC(O)-OH into $H_2O + CO_2$.

TABLE 3: Geometries for Species Involved in the HOCO + OH Reaction

species	coordinate	CCSD(T) cc-pVDZ	CCSD(T) cc-pVTZ
CO_2	r(CO)	1.174	1.166
OH	r(OH)	0.979	0.971
H_2O	r(OH)	0.966	0.959
	θ(HOH)	101.9	103.6
HOCO	r(O′H)	0.970	0.964
	r(CO′)	1.358	1.348
	r(CO)	1.191	1.182
	θ(HO′C)	105.9	107.1
	θ(O′CO)	126.6	127.0
	τ(HO′CO)	180.0	180.0
HOC(O)OH (cis, trans)	r(O′H)	0.971	0.965
	r(CO′)	1.363	1.357
	r(CO″)	1.203	1.197
	r(CO)	1.346	1.339
	r(OH)	0.970	0.964
	θ(O″CO′)	125.3	125.2
	θ(CO′H)	105.0	105.8
	θ(COH)	107.0	108.1
	τ(O″CO′H)	0.0	0.0
	τ(HOCO″)	180.0	180.0
$[HOC(O)OH \rightarrow H_2O + CO_2]^{\ddagger}$	r(C−O′)	1.272	1.265
	r(O′H)	1.237	1.245
	r(CO)	1.679	1.658
	r(OH)	0.973	0.966
	r(CO″)	1.182	1.175
	θ(O″CO′)	108.9	109.8
	θ(CO′H)	80.0	79.7
	θ(OCO′)	92.8	93.3
	θ(HOC)	145.4	145.2
	τ(HO′CO)	−3.5	−3.8
	τ(HOCO′)	180.2	180.3

from the addition of OH to HOCO must rotate into the (cis, trans) conformation in order to access the four-center TS to $H_2O + CO_2$. The heat of reaction for the production of H_2O and CO_2 from the (cis, trans)-HOC(O)OH intermediate is −4.9 kcal mol^{-1} at the CCSD(T)/cc-pVQZ//CCSD(T)/cc-pVTZ level of theory. Using the three-parameter complete-basis-set extrapolation procedure, this result is lowered to −5.3 kcal mol^{-1}. The barrier height is estimated to be 40.2 kcal mol^{-1} at the CBS−∞ limit. However, because the addition reaction exothermic by 108.1 kcal mol^{-1}, there is more than sufficient energy to overcome the four-center barrier for the HOC(O)OH reaction to $H_2O + CO_2$, thus making the OH + HOCO reaction effectively barrierless.

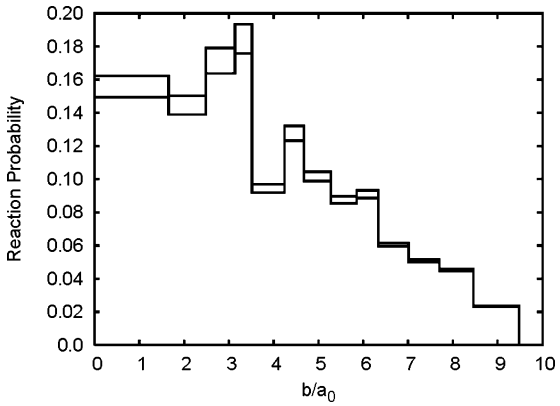

Figure 4. Opacity function for the total reaction probability of the OH + HOCO reaction calculated with all 2000 trajectories. The boxes indicate the statistical error bars.

To check the reliability of the calculations for the energetics, the heat of reaction for the $OH + HOCO \rightarrow H_2O + CO_2$ was examined. The heats of formation of all these species are well-known from the literature: OH (9.2 ± 0.3),[40] H_2O (−57.1 ± 0.01),[41] CO_2 (−93.97 ± 0.01),[41] and HOCO (−43.9 ± 0.5).[42] With these experimental heats of formation, the heat of reaction obtained is −116.0 ± 0.6 kcal mol^{-1}. From calculations at the CBS−∞ limit, we obtained −113.4 kcal mol^{-1}, which shows that the error in the calculated energetics is 2.6 kcal mol^{-1} and implies that the uncertainty in the energetics is ±3 kcal mol^{-1}. The calculations indicate that the major reaction pathway for the OH + HOCO reaction is the formation of $H_2O + CO_2$. Finally, a systematic comparison of the energetics is presented in Table 4. The SAC UMP2 method used in the dynamics calculations is seen to be consistent with the experimental results as well as the high-level ab initio calculations, thus justifying its use in this work.

D. Direct ab Initio Dynamics for the OH + HOCO Reaction. In the dynamics calculations, we have sampled five temperature points from 250 to 800 K. At each given temperature, 400 trajectories were run, yielding a total of 2000 trajectories. These were calculated several at a time on a cluster of PC−Linux workstations, one trajectory per CPU. Figure 4 shows the opacity function for the OH + HOCO reaction. Since the collision energies are not largely varying within the temperatures of simulation, we have combined data from all temperatures in plotting this figure. The maximum reactive impact parameter for this barrierless reaction is large. However, the reaction probability is only moderate, with values below 0.2 at all values of the impact parameter. Consequently, this is not a fast radical−radical reaction.

TABLE 4: Relative Energetics for the HOCO + OH Reaction

CCSD(T)	$OH + HOCO \rightarrow HOC(O)OH$	$HOC(O)OH \rightarrow H_2O + CO_2$	$OH + HOCO \rightarrow H_2O + CO_2$	$[HOC(O)OH \rightarrow H_2O + CO_2]^{\ddagger}$
cc-pVDZ	−101.7	−9.0	−110.7	39.2
cc-pVTZ	−105.9	−8.1	−114.0	39.6
cc-pVQZ	−107.2	−4.9	−112.1	40.2
CBS-∞	−108.1	−5.3	−113.4	40.2
SAC	−107.5	−9.3	−116.8	40.3
exptl			−116.0 ± 0.6	

TABLE 5: Dynamical Results for the OH + HOCO Reaction[a]

T/K	N_r	P_r	$10^{11} \times k(T)$
250	32	0.08	1.04 ± 0.18
300	29	0.0725	1.03 ± 0.18
400	33	0.0825	1.36 ± 0.23
500	27	0.0675	1.24 ± 0.23
800	32	0.08	1.86 ± 0.32

[a] $k(T)$ (cm^3 molecule^{-1} s^{-1}) is the thermal rate constant. N_r is the number of reactive trajectories over 400 trajectories for each temperature, and P_r is the reaction probability.

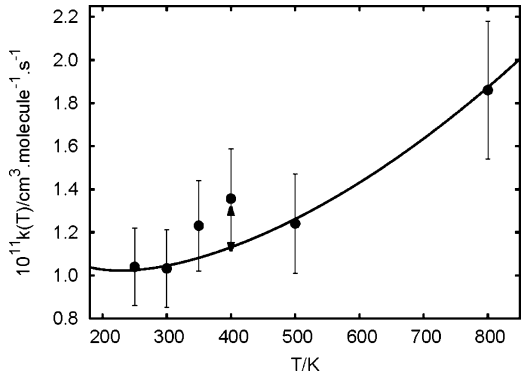

Figure 5. Calculated thermal rate constants (the filled circles with error bars) for the OH + HOCO reaction and the fitting curve (solid line). The triangles are extrapolated from the results of 300 K (upper triangle) and 500 K (down triangle).

Calculated thermal rate constants are given in Table 5. They have been fit by the functional form

$$k(T) = (a + bT^2)e^{-E_a/k_bT} \quad T \in [180, 850]\ \text{K}$$

with $a = 7.568\,05 \times 10^{-12}$ cm^3 molecule^{-1} s^{-1}, $b = 1.584\,84 \times 10^{-17}$ cm^3 molecule^{-1} s^{-1} K^{-2}, and $E_a = -0.089\,43$ kcal/mol. Since the value at $T = 400$ K seems somewhat larger than neighboring values, it was assigned a very small weight in the fitting procedure (see below). The final results are shown in Figure 5. At room temperature ($T = 300$ K), the thermal rate constant is predicted to be 1.03×10^{-11} cm^3 molecule^{-1} s^{-1}. The rate constant increases slowly then almost linearly with increasing temperature, but it is almost independent of T at low temperatures. Actually, this is not surprising for a barrierless reaction. The dipole−dipole interaction of the reactants may play an important role when the collision energy is small. Even if there is a negative activation energy (E_a) at low termperature, the temperature dependence of the rate constants should be weak. This prediction needs to be verified experimentally.

Since the error bar of the rate constant at $T = 400$ K just touches with the fitted curve, we have investigated this result in more detail. Two approaches were employed. One is the extrapolation approach, in which two rate constants at $T = 400$ K were estimated by reweighing the results sampled at the temperatures of 300 and 500 K. The values obtained are plotted in Figure 5 with the triangle symbols. The result extrapolated from 500 K falls on the fitted curve. The rate constant computed from the 300 K data still has a large deviation from the curve but within the statistical errors. This evidence suggests that there may be structure in the rate constant curve between the temperatures 300 and 400 K. To investigate such a possible structure, we have run an additional point at $T = 350$ K in the normal way with a total of 400 trajectories. The rate constant obtained is obviously larger than the fitted value, as shown in Figure 5. While it is quite possible that the "abnormal" behavior of the thermal rate constants near 400 K is correct, perhaps caused by a resonance state resulting from the long-range interaction, the deviations of the thermal rate constants are comparable to the statistical error bars, and it is hard to draw a definite conclusion based on our trajectory calculations.

It is interesting to study the reaction mechanism in detail. Figure 6 displays two typical reactive trajectories. A fast direct reaction trajectory is shown in Figure 6a. One can see that the hydrogen atom in OH likes to move toward the terminal oxygen

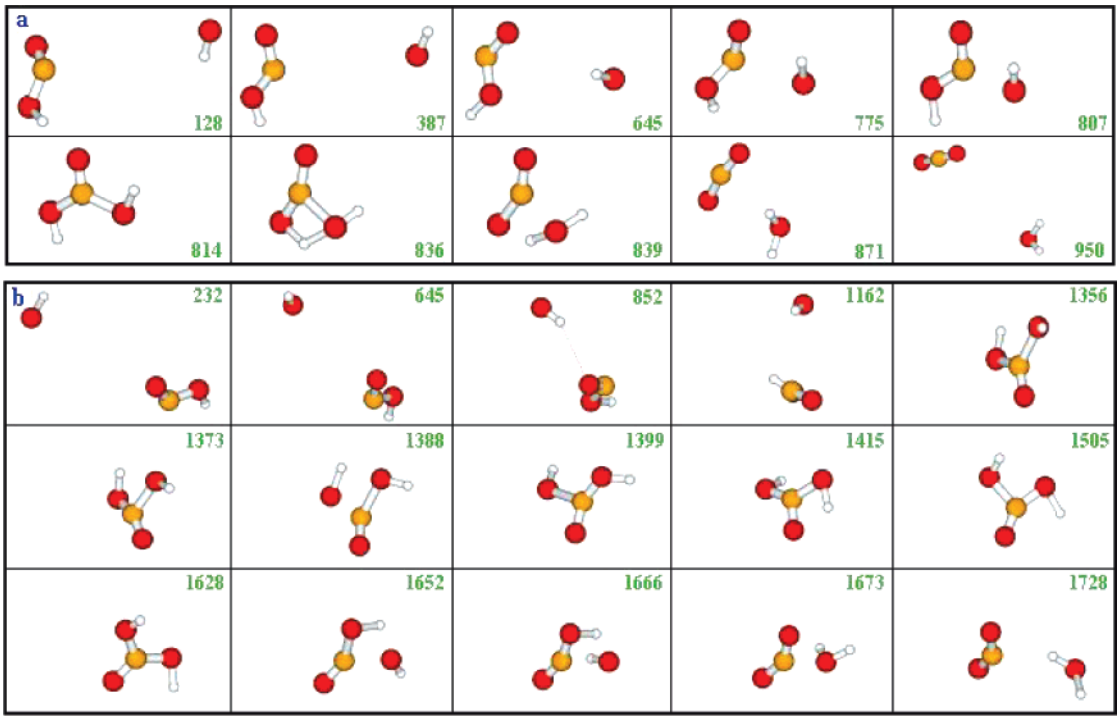

Figure 6. Two reactive trajectories for the OH + HOCO → H_2O + CO_2 reaction: (a) a fast reaction and (b) a somewhat slower reaction. The collision time in femtoseconds is indicated in each panel. For each trajectory, the orientation of each snapshot is kept the same.

of HOCO when the incident OH radical approaches the HOCO radical. This is due to an attractive hydrogen-bonding interaction. However, such a configuration does not lead to reaction. Instead, at a time of 807 fs, the OH molecule slightly rotates so that its oxygen atom can directly connect to the carbon atom in HOCO to form a strong C−O chemical bond. Since the intermediate HOC(O)OH is highly energized, the complex can easily overcome the transition state, as shown in the panel at $t = 836$ fs. After the HOCO hydrogen makes a 1,3-shift to the oxygen atom in the incoming OH molecule, the C−O bond quickly breaks to yield the $H_2O + CO_2$ products. The products are scattered in the backward hemisphere in this trajectory. The lifetime of the HOC(O)OH complex is as short as 30 fs. Therefore, it is a typical direct mechanism. Furthermore, because the HOC(O)OH complex has a nearly collinear OCO bond just before its dissociation (see the panel at $t = 836$ fs), it is expected that the bending vibrational mode of the CO_2 product will not be very excited. On the other hand, the products move apart swiftly so that the released energy is largely disposed as relative translational energy.

The trajectory in Figure 6b also shows that hydrogen bonding plays an important role during the early stages of the collision. A temporary hydrogen-bonded complex is formed at a time around 850 fs. After a while, this complex dissociates and becomes a loose OH + HOCO structure, as displayed in the $t = 1162$ panel. However, OH collides with HOCO once more to form a HOCOOH intermediate at $t = 1356$ fs. Then, the energized HOC(O)OH molecule undergoes large-amplitude vibrational motion for about 310 fs while rotating. Eventually, one OH fragment picks up the other H to yield the $H_2O + CO_2$ products at $t \approx 1670$ fs. Although the lifetime of the HOC(O)-OH intermediate in this trajectory is much longer than that in the trajectory in Figure 6a, the lifetime is still shorter than the rotational period of the molecule. Therefore, this trajectory is also an example of a direct reaction mechanism. In addition, one can clearly see that the dissociation does not proceed along the minimum energy path via the four-center transition state. This is a typical dynamical effect, especially for a reaction such as this with a transition state lying well below the reactants. As a result, the bending vibrational mode of both products is relatively hot. In this case, the products are forward scattered, which can be partially attributed to the large impact parameter in the initial conditions.

An important result of the present calculations is that at 300 K the estimated thermal rate constant for the OH + HOCO reaction to give H_2O and CO_2 is 1.03×10^{-11} cm^3 molecule^{-1} s^{-1}. When compared to the rates for reaction with O_2 + HOCO ($1.9 \pm 0.2 \times 10^{-12}$ cm^3 molecule^{-1} s^{-1})[18] and NO + HOCO ($2.45 \pm 0.2 \times 10^{-12}$ cm^3 molecule^{-1} s^{-1})[18] at 293 ± 2 K, the OH + HOCO reaction is predicted to be considerably faster. These results suggest that the OH + HOCO may in fact be an important removed mechanism for HOCO radicals. In the atmosphere, this reaction has been largely ignored. The present calculations provide a better appreciation for why the OH + HOCO reaction does not have much significance in the atmosphere, especially when considered in the context of abundances of species available for reaction. There is about a 12 orders-of-magnitude difference in the O_2 and OH abundances. Even if the OH + HOCO reaction rate is an order of magnitude faster than the O_2 + HOCO reaction, OH is unlikely to be competitive with O_2 for removing HOCO from the atmosphere. However, laboratory studies involving HOCO must take the OH + HOCO reaction into account, particularly, in those studies in which O_2 abundances are low. In addition, in comparison to the thermal rate constant (1.3×10^{-13} cm^3 molecule^{-1} s^{-1} at 298 K)[43] of the OH + CO reaction, the OH + HOCO reaction is also much faster. Therefore, this reaction may play an important role in removing OH radicals.

IV. Summary

Ab initio coupled-cluster calculations have been carried out to investigate the potential energy surface for the OH + HOCO reaction. The reaction is shown to proceed through an addition intermediate, HOC(O)OH, which then passes through a four-centered transition state as it produces the products H_2O and CO_2. The energetics suggest that the reaction is effectively barrierless. Direct ab initio dynamics calculations have shown that the rate for this reaction is relatively fast, and the rate constant may exhibit a near temperature-independence at lower temperatures, consistent with the formation of an intermediate complex, and a peak between 300 and 400 K. This reaction may be a major removal process for OH and HOCO radicals in combustion processes.

Acknowledgment. The work at Brookhaven National Laboratory was supported by the Division of Chemical Sciences, Office of Basic Energy Sciences of the U.S. Department of Energy under contract no. DE-AC02-98CH10886. We thank Professor I.W.M. Smith for valuable comments concerning this manuscript.

References and Notes

(1) Eston, R. E. *Chem. Rev.* **1995**, *99*, 2115.
(2) Ravishankara, A. R.; Thompson, R. L. *Chem. Phys. Lett.* **1983**, *99*, 377.
(3) Jonah, C. D.; Mulac, W. A.; Zeglinski, P. *J. Phys. Chem.* **1984**, *88*, 4100.
(4) Forster, R.; Frost, M.; Fulle, D.; Harmann, H. F.; Hippler, H.; Schlepegrell, A.; True, J. *J. Chem. Phys.* **1995**, *103*, 2949.
(5) Frost, M. J.; Sharkeley, P.; Smith, I. W. M. *J. Phys. Chem.* **1993**, *89*, 12254.
(6) Alagia, M.; Bulucani, N.; Casavecchia, P.; Stranges, D.; Volpi, G. G. *J. Chem. Phys.* **1993**, *98*, 8341.
(7) Jacox, M. E. *J. Chem. Phys.* **1988**, *88*, 4598.
(8) Radford, H. E.; Wei, W.; Sears, T. J. *J. Chem. Phys.* **1992**, *97*, 3989.
(9) Sears, T. J.; Farvzy, M. W.; Johnson, P. M. *J. Chem. Phys.* **1992**, *97*, 3996.
(10) Petty, J. T.; Moore, C. B. *J. Chem. Phys.* **1993**, *99*, 47.
(11) Miyoshi, A.; Matsui, H.; Wushida, N. *J. Chem. Phys.* **1994**, *100*, 3532.
(12) Ruscic, B.; Schwarz, M.; Birkowitz, J. *J. Chem. Phys.* **1989**, *91*, 6780.
(13) Milligan, D. E.; Jacox, M. E. *J. Chem. Phys.* **1971**, *54*, 927.
(14) DeMore, W. B. *Int. J. Chem. Kinet.* **1984**, *16*, 1187.
(15) Paragkeropoulous, G.; Irwin, R. S. *J. Chem. Phys.* **1984**, *80*, 259.
(16) Hufzumahaus, A.; Stuhl, F. *Ber. Bunsen Ger. Phys. Chem.* **1984**, *88*, 557.
(17) McCabe, D. C.; Gierczak, T.; Talukdar, R. K.; Ravishankara, A. R. *Geophys. Res. Lett.* **2001**, *28*, 3135.
(18) Petty, J. T.; Harrison, J. A.; Moore, C. B. *J. Chem. Phys.* **1993**, *97*, 11194.
(19) Olkhov, R. V.; Li, Q.; Osborne, M. C.; Smith, I. W. M. *Phys. Chem. Chem. Phys.* **2001**, *3*, 4522.
(20) Poggi, G.; Francisco, J. S. *J. Chem. Phys.* **2004**, *120*, 5073.
(21) Mielke, Z.; Olbert-Majkut, A.; Tokhadz, K. G. *J. Chem. Phys.* **2003**, *118*, 1364.
(22) Pople, J. A.; Head-Gordon, M.; Raghavachari, K. *J. Chem. Phys.* **1987**, *87*, 5968.
(23) Dunnins, T. H. J., Jr. *Chem. Phys.* **1989**, *93*, 1007.
(24) Kendell, R. A.; Dunning, T. H., Jr.; Harrison, R. J. *J. Chem. Phys.* **1992**, *96*, 6796.
(25) Schlegel, H. B. *J. Comput. Chem.* **1982**, *3*, 214.
(26) Raghavachari, K.; Twiks, G. W.; Pople, J. A.; Head-Gordon, M. *Chem. Phys. Lett.* **1989**, *157*, 479.
(27) Watts, J. D.; Gauss, J.; Bartlett, R. J. *J. Chem. Phys.* **1993**, *98*, 8718.

(28) Peterson, K. A.; Woon, D. W.; Dunning, T. H., Jr. *J. Chem. Phys.* **1994**, *100*, 7410.
(29) Yu, H.-G.; Muckerman, J. T. *J. Phys. Chem. A* **2004**, *108*, 8615.
(30) Yu, H.-G.; Muckerman, J. T. *J. Phys. Chem. A* **2005**, *109*, 1890.
(31) Hase, W. L. In *Encyclopedia of Computational Chemistry*; Schleyer, P. v. R., Ed.; John Wiley & Sons: New York, 1998.
(32) Faist, M. B.; Muckerman, J. T.; Schubert, F. E. *J. Chem. Phys.* **1978**, *69*, 4087.
(33) Muckerman, J. T.; Faist, M. B. *J. Phys. Chem.* **1979**, *83*, 79.
(34) Wilson, R. J. *Introduction to Graph Theory*; Longman: London, 1972.
(35) West, D. B. *Introduction to Graph Theory*; Prentice Hall: Englewood Cliffs, NJ, 1996.
(36) Gordon, M. S.; Truhlar, D. G. *J. Am. Chem. Soc.* **1986**, *108*, 5412.
(37) Gordon, M. S.; Truhlar, D. G. *Int. J. Quantum Chem.* **1987**, *31*, 81.
(38) Gordon, M. S.; Nguyen, K. A.; Truhlar, D. G. *J. Phys. Chem.* **1989**, *93*, 7356.
(39) Frisch, M. J.; Trucks, G. W.; Schlegel, H. B.; Scuseria, G. E.; Robb, M. A.; Cheeseman, J. R.; Montgomery, Jr., J. A.; Vreven, T.; Kudin, K. N.; Burant, J. C.; Millam, J. M.; Iyengar, S. S.; Tomasi, J.; Barone, V.; Mennucci, B.; Cossi, M.; Scalmani, G.; Rega, N.; Petersson, G. A.; Nakatsuji, H.; Hada, M.; Ehara, M.; Toyota, K.; Fukuda, R.; Hasegawa, J.; Ishida, M.; Nakajima, T.; Honda, Y.; Kitao, O.; Nakai, H.; Klene, M.; Li, X.; Knox, J. E.; Hratchian, H. P.; Cross, J. B.; Bakken, V.; Adamo, C.; Jaramillo, J.; Gomperts, R.; Stratmann, R. E.; Yazyev, O.; Austin, A. J.; Cammi, R.; Pomelli, C.; Ochterski, J. W.; Ayala, P. Y.; Morokuma, K.; Voth, G. A.; Salvador, P.; Dannenberg, J. J.; Zakrzewski, V. G.; Dapprich, S.; Daniels, A. D.; Strain, M. C.; Farkas, O.; Malick, D. K.; Rabuck, A. D.; Raghavachari, K.; Foresman, J. B.; Ortiz, J. V.; Cui, Q.; Baboul, A. G.; Clifford, S.; Cioslowski, J.; Stefanov, B. B.; Liu, G.; Liashenko, A.; Piskorz, P.; Komaromi, I.; Martin, R. L.; Fox, D. J.; Keith, T.; Al-Laham, M. A.; Peng, C. Y.; Nanayakkara, A.; Challacombe, M.; Gill, P. M. W.; Johnson, B.; Chen, W.; Wong, M. W.; Gonzalez, C.; Pople, J. A. *Gaussian 03*, Revision B.04; Gaussian, Inc., Wallingford CT, 2004.
(40) Rusic, B.; Wagner, A. F.; Harding, L. B.; Ashar, R. L.; Feller, D.; Dixon, D. A.; Peterson, K. A.; Song, Y.; Qian, X. M.; Ng, C. Y.; Liu, J. B.; Chem, W. W. *J. Phys. Chem. A* **2002**, *106*, 2727.
(41) Chase, W. W., Jr.; Davies, C. A.; Downey, R., Jr.; Frarip, D. J.; McDonald, R. A.; Syvervnd, A. N. *J. Phys. Chem. Ref. Data, Suppl.* **1985**, *1*, 14.
(42) Feller, D.; Dixon, D. A.; Francisco, J. S. *J. Chem. Phys. A* **2003**, *107*, 1604.
(43) Atkinson, R.; Baulch, D. L.; Cox, R. A.; Hampson, R. F., Jr.; Kerr, J. A.; Ross, M. J.; Troe, J. *J. Phys. Chem. Ref. Data* **1999**, *28*, 191.